

c.1



# RESEARCH MEMORANDUM

INVESTIGATION OF TRANSONIC FLUTTER CHARACTERISTICS OF A  
THIN  $10^\circ$  SWEEPBACK WING HAVING AN ASPECT RATIO OF 4  
AND A TAPER RATIO OF 0.6

By George W. Jones, Jr. ✓

Langley Aeronautical Laboratory  
Langley Field, Va.

CLASSIFICATION CHANGE  
UNCLASSIFIED

LIBRARY COPY

FEB 15 1957

LANGLEY AERONAUTICAL LABORATORY  
LIBRARY, NASA  
LANGLEY FIELD, VIRGINIA

Authority of *Nasa PA 4*  
*Effective*  
*Date 2-10-59*  
*NB 4-1-59*

CLASSIFIED DOCUMENT

This material contains information affecting the National Defense of the United States within the meaning of the espionage laws, Title 18, U.S.C., Secs. 793 and 794, the transmission or revelation of which in any manner to an unauthorized person is prohibited by law.

## NATIONAL ADVISORY COMMITTEE FOR AERONAUTICS

WASHINGTON  
February 8, 1957



UNCLASSIFIED



## NATIONAL ADVISORY COMMITTEE FOR AERONAUTICS

## RESEARCH MEMORANDUM

INVESTIGATION OF TRANSONIC FLUTTER CHARACTERISTICS OF A  
THIN  $10^\circ$  SWEEPBACK WING HAVING AN ASPECT RATIO OF 4  
AND A TAPER RATIO OF 0.6

By George W. Jones, Jr.

## SUMMARY

A flutter investigation has been made in the Langley transonic blow-down tunnel at Mach numbers between 0.79 and 1.34 on a thin  $10^\circ$  sweptback wing having an aspect ratio of 4 and a taper ratio of 0.6. The data obtained have been compared with data from NACA Research Memorandum L55113a for  $0^\circ$  and  $30^\circ$  sweptback wings with the same aspect ratio and taper ratio. The results indicated that for wings of the type investigated, the flutter boundary for the  $10^\circ$  sweptback wing falls between those for the  $0^\circ$  and  $30^\circ$  sweptback wings in the low supersonic Mach number range. However, the subsonic level (around a Mach number of 0.8) of the flutter boundary for the  $10^\circ$  sweptback wing lies above those for the  $0^\circ$  and  $30^\circ$  sweptback wings. In addition, the amount of rise in the flutter boundary from the subsonic level to supersonic values is about the same for the wings with angles of sweepback of  $10^\circ$  and  $0^\circ$ , but is much greater for the wing with an angle of sweepback of  $30^\circ$ .

## INTRODUCTION

Among the plan forms for which transonic flutter data were presented in reference 1 were a series of thin wings having an aspect ratio of 4, a taper ratio of 0.6, streamwise NACA 65A004 airfoil sections, and sweepback angles from  $0^\circ$  to  $60^\circ$ . For each of these plan forms the flutter-speed ratios (ratio of the experimental flutter speed to the flutter speed calculated by using two-dimensional incompressible aerodynamic coefficients) increased with Mach number from a Mach number of about 0.9 up to at least 1.3. The amount of increase was least for the wing with an angle of sweepback of  $60^\circ$  and progressively greater for wings with angles of sweepback of  $52.5^\circ$ ,  $45^\circ$ , and  $30^\circ$ . A reversal of this trend was shown for the wing with an angle of sweepback of  $0^\circ$  which had less increase in flutter-speed ratio in the supersonic region than either the  $30^\circ$  or  $45^\circ$  sweptback wings.

CONFIDENTIAL

UNCLASSIFIED

Because of the decided reversal in trend between sweepback angles of  $30^\circ$  and  $0^\circ$ , the question has arisen as to what would be the variation of flutter-speed ratio with Mach number for a similar wing with only a small amount of sweepback. In order to supply this information, the present limited investigation was undertaken in the Langley transonic blowdown tunnel to determine the transonic flutter characteristics of a  $10^\circ$  sweptback wing with an aspect ratio of 4, a taper ratio of 0.6, and streamwise NACA 65A004 airfoil sections. Experimental flutter data were obtained for this wing at several Mach numbers from 0.79 to 1.34. Reference flutter speeds were calculated in the same manner as in reference 1 and were used to obtain flutter-speed ratios for comparison with the data of reference 1.

## SYMBOLS

- A aspect ratio of wing including body intercept,  $\frac{\text{Span}^2}{\text{Area}}$
- a distance in wing semichords from midchord to elastic axis position; perpendicular to quarter-chord line, positive with elastic axis behind midchord,  $2x_0 - 1$
- $A_g$  geometric aspect ratio,  $\frac{(\text{Exposed semispan})^2}{\text{Exposed semispan area}}$
- b half-chord perpendicular to quarter-chord line, ft
- $b_r$  half-chord perpendicular to quarter-chord line at intersection of quarter-chord line and wing root, ft
- $b_s$  half-chord measured streamwise at intersection of wing and fuselage, ft
- EI bending stiffness, lb-in.<sup>2</sup>
- GJ torsion stiffness, lb-in.<sup>2</sup>
- $f_{h,i}$  measured coupled bending frequencies, ( $i = 1, 2, \text{ or } 3$ ), cps
- $f_t$  measured first coupled torsion frequency, cps
- $f_\alpha$  uncoupled first torsion frequency,

$$f_\alpha = f_t \left[ 1 - \frac{(x_\alpha/r_\alpha)^2}{1 - (f_{h,1}/f_t)^2} \right]^{1/2}, \quad (\text{values taken at } \eta = 0.75),$$

cps

$g$	structural damping coefficient
$g_h$	measured structural damping coefficient in first bending
$g_\alpha$	structural damping coefficient in torsion
$I_\alpha$	wing mass moment of inertia per unit length along quarter-chord line, measured about elastic axis, slug-ft <sup>2</sup> /ft
$k$	reduced frequency, $b\omega/V_n$
$l$	length of exposed quarter-chord line of a wing panel, ft
$M$	Mach number
$m$	mass of wing per unit length along quarter-chord line, slugs/ft
$q$	dynamic pressure, lb/sq ft
$r_\alpha$	nondimensional radius of gyration of wing about elastic axis, $(I_\alpha/mb^2)^{1/2}$
$V$	airstream velocity, ft/sec
$V_e/V_R$	flutter-speed ratio, ratio of experimental flutter speed to calculated reference flutter speed
$V_n$	component of airstream velocity normal to quarter-chord line, $V \cos \Lambda$ , ft/sec
$x_o$	distance of elastic axis of wing section behind leading edge in fraction of chord, both measured perpendicular to quarter-chord line
$x_\alpha$	distance in semichords from wing elastic axis to wing center of gravity (measured perpendicular to quarter-chord line), positive with center of gravity behind elastic axis
$\eta$	nondimensional coordinate along quarter-chord line, fraction of length $l$
$\mu$	mass-ratio parameter, $\frac{m}{\pi\rho b^2}$
$\lambda$	taper ratio of wing, $\frac{\text{Streamwise tip chord}}{\text{Chord in plane of symmetry}}$

$\Lambda$	angle of sweepback of wing quarter-chord line, deg
$\rho$	air density, slugs/cu ft
$\omega$	angular frequency of flutter, radians/sec
$\omega_{h,i}$	angular bending frequency, $2\pi f_{h,i}$ , radians/sec
$\omega_{\alpha}$	angular uncoupled first torsion frequency, $2\pi f_{\alpha}$ , radians/sec

## Subscripts:

e	experimental values
R	calculated values

## MODELS

The wing of the present investigation had a sweepback angle of  $10^{\circ}$  along the quarter-chord line, an aspect ratio of 4, a taper ratio of 0.6, NACA 65A004 streamwise airfoil sections, and a ratio of sting-fuselage diameter to wing span of 0.22. The model wing panels were connected by a mounting block which fitted flush with the sting-fuselage and was an integral part of the wing. (See fig. 1.) In accordance with the three-digit designation code of reference 1, this wing is designated a 410 wing (the first digit is the aspect ratio to the nearest integer and the last two digits give the sweepback angle in degrees). The basic dimensions of the model are shown in figure 1.

Because of the destruction of the models by flutter, three models were needed to obtain the desired data. The models were constructed of solid Consoweld (ref. 2), a phenolic laminate material with high-strength paper reinforcement.

Measurements were made of the following physical parameters on each wing panel of each model: elastic axis position, structural damping coefficient in bending, and the first four coupled natural frequencies and the node lines associated with the second, third, and fourth coupled frequencies. The frequencies and node lines which were measured are presented in figure 2. On the right panel of model 3 the spanwise variations of the following parameters were determined and are presented in table I: mass, center-of-gravity location, and the square of the radius of gyration (taken about elastic axis). Also presented in table I are certain basic wing geometric parameters which were the same for all models; for each panel of each model a tabulation is given of the lower

frequencies, frequency ratios, and the structural damping coefficient in bending. The spanwise variations of bending and torsion stiffnesses ( $EI$  and  $GJ$ , respectively) were also measured on the right panel of model 3 and are presented in figure 3. The parameters measured on only the right panel of model 3 are used as representative values for all of the panels. A discussion of the methods used to measure the physical parameters may be found in references 1 and 3.

#### APPARATUS AND TESTS

A detailed description of the tunnel, the test instrumentation and the testing techniques may be found in reference 1. Excellent agreement between flutter data obtained in the tunnel and in free air is shown in reference 4. In the following paragraphs only the salient features of the apparatus and tests are given.

The tests were made in the Langley transonic blowdown tunnel which has a slotted, octagonal test section measuring 26 inches between flats. During the operation of the tunnel a preselected Mach number, which is determined by the size of the opening in an orifice plate, can be held approximately constant (after the orifice is choked) while test-section stagnation pressure (and thus density) is varied. The tunnel can operate from subsonic Mach numbers through the transonic range and up to a supersonic Mach number of about 1.40. The density range of the tunnel is from approximately 0.001 to 0.012 slug per cubic foot.

The flutter wings were cantilever mounted at an angle of attack of  $0^\circ$  in a cylindrical sting fuselage which covers the mounting block. This sting extends upstream into the subsonic flow region of the tunnel without change in diameter. Thus, the formation of a bow shock wave which might reflect from the tunnel walls onto the model is prevented. The fundamental frequency of the support system is approximately 15 cycles per second, and its weight is 289 pounds.

Basically, the instrumentation was as follows: Wire strain gages, installed near each panel root, were used to indicate the bending and torsion motions of the wing. A recording oscillograph was used to give a continuous record of the strain-gage signals, tunnel stagnation temperature and pressure, and test-section static pressure. The record of the strain-gage signals was used to determine the start of flutter and the frequency of wing oscillations.

Flutter speeds and flutter frequencies were determined for the wing at several Mach numbers throughout the transonic range from 0.79 to 1.34.

## RESULTS

## Analysis

The data obtained in the present investigation are presented as the variation of flutter-speed ratio (ratio of experimental flutter speed to a calculated reference flutter speed) with Mach number. The method of calculating the reference flutter speeds is the same as that of reference 1 which was based on the analysis of reference 5. Briefly, two-dimensional incompressible aerodynamic coefficients, based on the component of the airstream velocity normal to the quarter-chord line, were employed in a modal type of analysis. The spanwise derivative of the velocity potential appearing in the method of reference 5 was neglected. In the analysis the flutter mode shape was approximated by the superposition of the first two uncoupled free-vibration mode shapes of a uniform cantilever beam. Studies made in reference 1 indicated that, for the 410 wing, which had a ratio of second bending to first torsion frequency of about 1.1, the addition of a third mode might have a significant effect on the reference flutter speed. As a check, a second reference flutter-speed analysis was made in which the flutter mode shape was approximated by the superposition of the first three uncoupled free-vibration mode shapes of a uniform cantilever beam.

The effective wing root and tip are defined in the present analysis as the perpendiculars to the quarter-chord line of the intersections of the quarter-chord line with the actual root and tip, respectively.

The values of  $k$  were weighted along the span in accordance with the wing taper, and the spanwise variations of the Theodorsen functions  $F(k)$  and  $G(k)$  were approximated by a straight line between the root and tip values.

The solution of the flutter stability determinant was obtained in the form of structural damping coefficient  $g$  as a function of  $V_n/b_r\alpha_\alpha$ . The structural damping coefficient used was that measured in bending with the assumption that  $g_h = g_\alpha = g$ .

## General Comments

In some instances the two wing panels of the same model did not flutter simultaneously. For such cases a separate data point for the occurrence of flutter on each panel is presented in the tables and figures.

An easily defined start of flutter was not always obtained. Often, a period of intermittent sinusoidal-type oscillations in bending and torsion preceded continuous flutter and obscured the exact start of flutter. Such periods are designated low-damping regions as in reference 1, since the sum of the aerodynamic and structural damping is near zero.

Where low damping occurred, two data points were picked - one near the start of the low-damping region and the other near the start of continuous flutter. Both data points are presented in the tables and figures.

### Presentation of Data

The experimental and analytical results of this investigation are presented in table II. The analytical results are from the two-mode computations of reference flutter-speed values. In this table the first five columns describe chronologically the flutter behavior of each wing panel during each tunnel run (a run is defined as one operation of the wind tunnel from valve opening to valve crossing). The first column gives the model identification number, the second column the run number, and the third column the chronological number of each data point during each run. The fourth and fifth columns contain code letters which describe the behavior of the wing panels at the time of each data point. Definitions of the code letters are given at the top of table II.

The experimental flutter data obtained for the 410 wing and faired curves for the 400 and 430 wings of reference 1 are shown in figure 4 in the form of a plot of the parameter  $\frac{V_e}{b_s \omega_\alpha \sqrt{\mu_e}}$  as a function of Mach number. In this figure and in figures 5 and 6 the low-damping regions are indicated by dashed lines which extend from the start-of-low-damping point (marked only by the end of the dashed line) to the continuous-flutter point (marked by a symbol at the upper end of the dashed line).

The experimental flutter data normalized by calculated results are presented as functions of Mach number in figures 5 to 7. Figure 5 presents the flutter-speed ratios obtained on the 410 wing with both two and three degrees of freedom. Figure 6 compares the flutter-speed ratios for the 410 wing with the flutter-speed ratios for the 400 and 430 wings from reference 1. Figure 7 shows the faired flutter-speed ratio boundaries for the wing of the present investigation and for all the wings of reference 1 which had aspect ratios of 4 and taper ratios of 0.6.

## DISCUSSION

The experimental data obtained for the 410 wing and presented in figure 4 show that up to a Mach number of 1.2 the data obtained for the three different models are in good agreement. Above a Mach number of 1.2 some scatter is shown, and in drawing the flutter boundary through the scatter, the data obtained (see table II) for the one wing panel of model 1 and the two panels of model 2 are favored over those obtained for the one panel of model 3. The flutter boundary in this region is not as definitely defined as at the lower Mach numbers and is shown in figures as a dotted line.

A comparison of the faired flutter boundary for the 410 wing with the boundaries for the 400 and 430 wings of reference 1 (see fig. 4) indicates that in the low supersonic range the 410 wing flutter boundary lies between those for the 400 and 430 wings. The slope of the 410 wing boundary in this range is slightly less than that for the 400 wing. Also, the subsonic level of the boundary for the 410 wing is slightly above that for the 400 wing and considerably above that for the 430 wing. If the overall increase in the parameter  $\frac{V_e}{b_s \omega_\alpha \sqrt{\mu_e}}$  from subsonic to supersonic Mach numbers is considered, the 410 and 400 wings increase by about the same amount but there is a much larger increase for the 430 wing.

Figure 5 shows for the 410 wing no significant differences between the reference flutter speeds calculated with the two-mode analysis and those calculated with the three-mode analysis. The subsonic level of the flutter boundary obtained ( $V_e/V_R$  values near 1.1 at a Mach number of 0.8) shows the reference flutter speeds for the 410 wing to be somewhat conservative. The flutter-speed ratios increase steadily with Mach numbers above 0.85 to a  $V_e/V_R$  value of 1.48 at a Mach number of 1.3.

Figure 6 shows that, at low supersonic Mach numbers, the 410 wing flutter-speed ratios fall between those for the 400 and 430 wings. The data in this figure are based on reference flutter speeds calculated with two-mode analyses. The rate of rise of  $V_e/V_R$  for the 410 wing in this Mach number range appears to be slightly less than that of the 400 wing. At Mach numbers around 0.8 the level of the 410 wing  $V_e/V_R$  curve is about 10 percent higher than that of the 400 wing and about 7 percent higher than that of the 430 wing curve, although the fairing of the 430 wing curve in this area may be somewhat arbitrary. The amount of increase in flutter-speed ratio from the subsonic level (Mach numbers around 0.8) to supersonic values is about the same for the 410 and 400 wings, but there is a much larger increase for the 430 wing. The faired flutter boundaries of figure 6 are shown in figure 7 with those for similar wings of reference 1 having aspect ratios of 4, taper ratios

of 0.6, and sweepback angles of  $45^\circ$ ,  $52.5^\circ$ , and  $60^\circ$ . As discussed in reference 1, the reference flutter speeds for the wings with sweepback angles less than  $45^\circ$  were computed by a two-mode analysis whereas the  $45^\circ$ ,  $52.5^\circ$ , and  $60^\circ$  wing reference flutter speeds were computed by a three-mode analysis.

### CONCLUSIONS

Transonic flutter data obtained on a thin  $10^\circ$  sweptback wing having an aspect ratio of 4 and a taper ratio of 0.6 have been compared with data from NACA Research Memorandum L55113a for  $0^\circ$  and  $30^\circ$  sweptback wings with the same aspect ratio and taper ratio, and the following conclusions have been drawn:

1. For wings of the type investigated, flutter boundaries in the form of flutter-speed ratio against Mach number and an experimental parameter consisting of the reduced frequency divided by the square root of the mass ratio show that, in the low supersonic Mach number range, the flutter boundary for the  $10^\circ$  sweptback wing falls between those for the  $0^\circ$  and  $30^\circ$  wings. However, the subsonic level (around Mach number 0.8) of the flutter boundary for the  $10^\circ$  sweptback wing lies above those for the  $0^\circ$  and  $30^\circ$  sweptback wings.

2. The amount of rise in the flutter boundary from the subsonic level to low supersonic values is about the same for the wings with angles of sweepback of  $10^\circ$  and  $0^\circ$  but is much greater for the wing with an angle of sweepback of  $30^\circ$ .

Langley Aeronautical Laboratory,  
National Advisory Committee for Aeronautics,  
Langley Field, Va., November 29, 1956.

## REFERENCES

1. Unangst, John R., and Jones, George W., Jr.: Some Effects of Sweep and Aspect Ratio on the Transonic Flutter Characteristics of a Series of Thin Cantilever Wings Having a Taper Ratio of 0.6. NACA RM L55I13a, 1956.
2. Lamb, J. J., Boswell, Isabelle, and Axilrod, B. M.: Tensile and Compressive Properties of Laminated Plastics at High and Low Temperatures. NACA TN 1550, 1948.
3. Land, Norman S., and Abbott, Frank T., Jr.: Transonic Flutter Investigation of a Fighter-Airplane Wing Model and Comparison With a Systematic Plan-Form Series. NACA RM L55B16, 1955.
4. Bursnall, William J.: Initial Flutter Tests in the Langley Transonic Blowdown Tunnel and Comparison With Free-Flight Flutter Results. NACA RM L52K14, 1953.
5. Barmby, J. G., Cunningham, H. J., and Garrick, I. E.: Study of the Effects of Sweep on the Flutter of Cantilever Wings. NACA Rep. 1014, 1951. (Supersedes NACA TN 2121.)

TABLE I.- PHYSICAL PROPERTIES OF MODELS

Parameter	Models 1, 2, and 3	$\eta$	Model 3 (right panel)				
			$x_\alpha$	a	$r_\alpha^2$	m	b/b <sub>r</sub>
NACA section	65A004	0.05	-0.122	0.047	0.252	0.00872	0.98285
A	4	.15	-.103	.020	.221	.00794	.94855
$\Lambda$ , deg	10	.25	-.081	-.009	.209	.00721	.91425
$\lambda$	0.6	.35	-.058	-.037	.215	.00654	.87995
Panel $\lambda$	0.657	.45	-.030	-.066	.204	.00595	.84565
Span, ft	1.142	.55	.002	-.095	.227	.00540	.81135
$A_g$	1.65	.65	.035	-.122	.234	.00496	.77705
l, ft	0.453	.75	.067	-.149	.240	.00455	.74275
b <sub>r</sub> , ft	0.165	.85	.091	-.177	.247	.00417	.70845
b <sub>s</sub> , ft	0.163	.95	.114	-.205	.242	.00384	.67415

Frequency	Model 1		Model 2		Model 3	
	Left panel	Right panel	Left panel	Right panel	Left panel	Right panel
$f_{h,1}$	117	112	115	115	112	116
$f_{h,2}$	510	493	505	505	496	507
$f_{h,3}$	1470	1420	1425	1440	1400	1450
ft	468	468	470	467	459	468
$f_\alpha$	463	463	465	462	454	463
$\omega_{h,1}/\omega_\alpha$	.2527	.2419	.2473	.2489	.2467	.2505
$\omega_{h,2}/\omega_\alpha$	1.1015	1.0648	1.0860	1.0931	1.0925	1.0950
$g_h$	.016	.015	.023	.022	.034	.043

TABLE II.- COMPILATION OF EXPERIMENTAL AND ANALYTICAL RESULTS

[Wing-panel-behavior code:  
 F - flutter  
 N - no flutter  
 D - low damping  
 X - wing panel destroyed  
 G - strain gages inoperative]

Model	Run	Point	Wing panel behavior		M <sub>e</sub>	V <sub>e</sub> /V <sub>R</sub>	ρ <sub>e</sub> , slugs cu ft	μ <sub>e</sub> (a)	α <sub>U</sub> , radians sec	α <sub>R</sub> , radians sec	α <sub>e</sub> , radians sec	α <sub>e</sub> /α <sub>R</sub>	V <sub>e</sub> , ft/sec	V <sub>R</sub> , ft/sec	V <sub>e</sub> / b <sub>R</sub> α <sub>U</sub>	V <sub>R</sub> / b <sub>R</sub> α <sub>U</sub>	q <sub>e</sub> , lb/ft <sup>2</sup>	V <sub>e</sub> / b <sub>R</sub> α <sub>U</sub> √μ <sub>e</sub>	b <sub>R</sub> α <sub>e</sub> / V <sub>e</sub> cos Λ
			Left	Right															
1	1	1	D	D	0.942	1.090	0.0040	24.23	2911	----	----	970.6	890.5	2.02	1.85	1878	0.4156	-----	
1	1	2	F	F	.936	1.120	.0043	22.25	2911	1606	1213	0.755	961.7	858.8	2.00	1.79	2006	.4297	0.2113
1	2	1	F	X	1.237	1.409	.0043	22.47	2911	1601	1288	.804	1215.5	862.6	2.53	1.80	3172	.5404	.1775
1	3	1	D	X	.873	1.109	.0050	19.45	2911	----	----	899.8	811.2	1.87	1.69	2009	.4300	-----	
1	3	2	F	X	.885	1.160	.0054	17.99	2911	1645	1162	.706	910.5	784.8	1.90	1.63	2223	.4524	.2138
2	4	1	D	D	1.154	1.272	.0039	24.74	2914	----	----	1145.2	900.2	2.38	1.87	2559	.4846	-----	
2	4	2	F	F	1.161	1.314	.0042	22.83	2914	1587	1294	.815	1142.8	869.4	2.38	1.81	2763	.5035	.1897
2	5	1	D	D	1.123	1.219	.0034	28.70	2914	----	----	1165.1	956.0	2.42	1.99	2284	.4595	-----	
2	5	2	F	F	1.112	1.239	.0038	25.66	2914	1562	1175	.752	1132.9	914.2	2.36	1.90	2413	.4707	.1738
2	6	1	D	D	1.060	1.182	.0040	24.20	2914	----	----	1053.7	891.1	2.19	1.85	2216	.4509	-----	
2	6	2	F	D	1.058	1.240	.0045	21.27	2924	1600	1191	.744	1047.6	844.3	2.17	1.75	2491	.4766	.1905
2	6	3	F	F	1.064	1.260	.0047	20.53	2905	1610	1216	.755	1046.9	831.1	2.18	1.73	2576	.4879	.1946
2	7	1	D	N	1.282	1.365	.0038	25.42	2924	----	----	1243.5	910.9	2.58	1.89	2936	.5174	-----	
2	7	2	F	D	1.282	1.432	.0043	22.49	2914	1590	1363	.857	1237.0	863.7	2.57	1.80	3286	.5491	.1846
2	7	3	F	F	1.275	1.454	.0045	21.30	2905	1603	1395	.870	1226.9	844.1	2.56	1.76	3413	.5614	.1905
2	8	1	D	D	1.180	1.238	.0035	27.89	2914	----	----	1173.5	947.8	2.44	1.97	2583	.4677	-----	
2	8	2	F	D	1.170	1.290	.0039	24.45	2924	1571	1247	.794	1156.2	895.9	2.40	1.86	2640	.4906	.1807
2	8	3	F	F	1.181	1.328	.0042	23.01	2905	1588	1257	.792	1158.2	871.9	2.42	1.82	2815	.5099	.1818
2	9	1	D	D	1.032	1.138	.0035	27.06	2914	----	----	1064.7	935.3	2.21	1.94	1978	.4308	-----	
2	9	2	F	F	1.027	1.168	.0038	25.12	2914	1567	1118	.714	1057.8	906.0	2.20	1.88	2150	.4443	.1771
2	10	1	D	G	.862	1.055	.0045	21.30	2924	----	----	891.0	844.3	1.85	1.75	1798	.4051	-----	
2	10	2	F	G	.876	1.096	.0048	20.02	2924	1612	1116	.692	901.1	822.6	1.87	1.70	1958	.4226	.2075
3	11	1	D	D	.788	1.070	.0057	16.95	2883	----	----	824.2	770.6	1.73	1.62	1935	.4260	-----	
3	11	2	F	F	.790	1.098	.0061	15.89	2883	1626	1257	.773	824.1	750.2	1.73	1.58	2064	.4400	.2556
3	12	1	D	G	1.340	1.286	.0030	31.70	2855	----	----	1290.7	1003.9	2.74	2.13	2536	.4926	-----	
3	12	2	F	G	1.337	1.358	.0035	27.51	2855	1528	1326	.868	1283.1	945.0	2.72	2.01	2889	.5257	.1731
3	13	1	D	G	1.323	1.254	.0029	32.93	2855	----	----	1278.4	1019.4	2.71	2.16	2396	.4788	-----	
3	13	2	F	G	1.339	1.351	.0034	28.00	2855	1524	1319	.865	1286.5	952.0	2.73	2.02	2853	.5224	.1718
3	14	1	D	G	1.220	1.212	.0031	31.28	2855	----	----	1210.5	998.7	2.57	2.12	2262	.4651	-----	
3	14	2	F	G	1.235	1.251	.0033	29.53	2855	1514	1269	.838	1218.5	974.2	2.59	2.07	2426	.4818	.1745

<sup>a</sup>Values taken at 0.75η station.

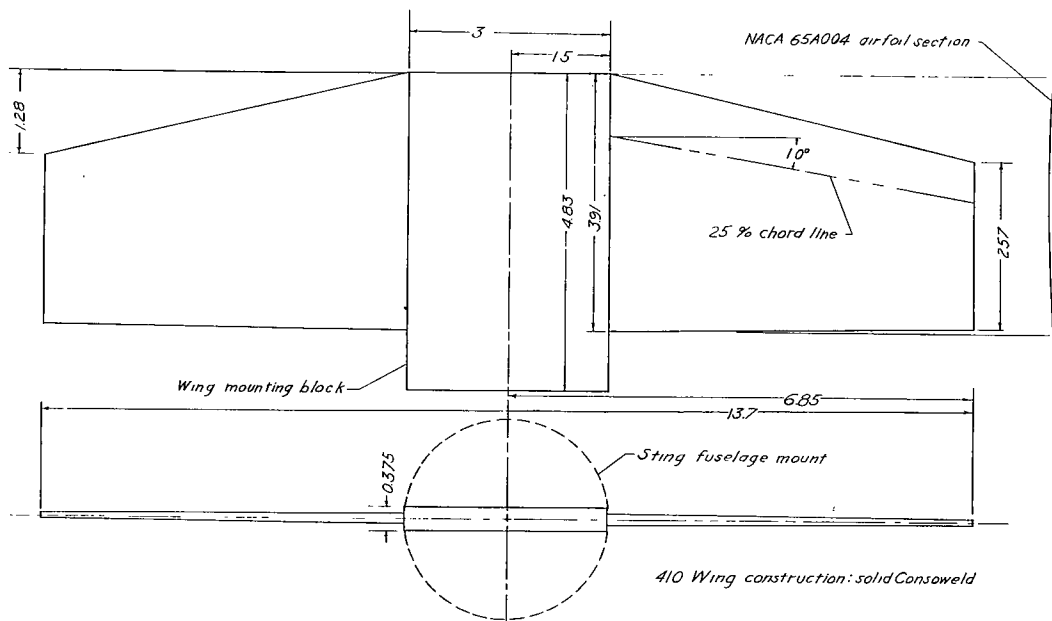


Figure 1.- Sketch of 410 wing showing basic model dimensions and construction. All dimensions are in inches.

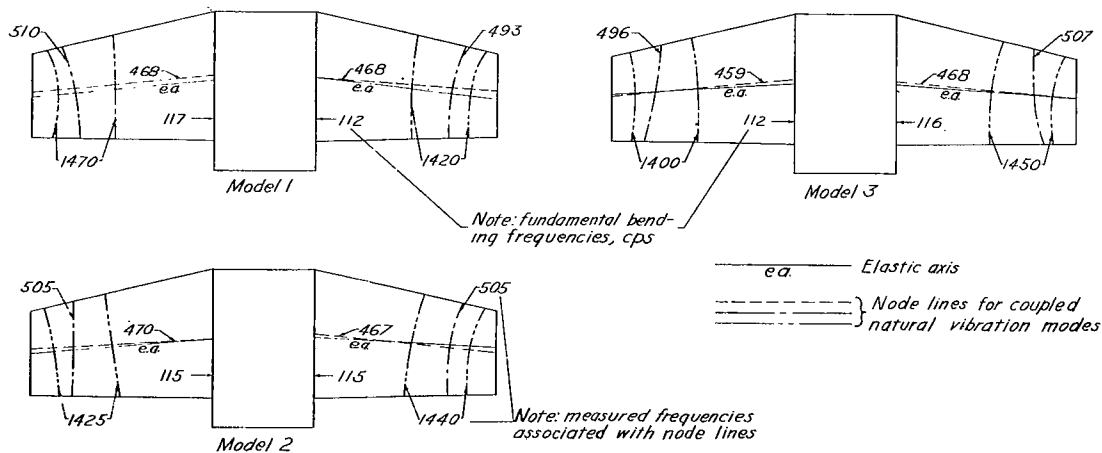


Figure 2.- Coupled natural vibration frequencies, elastic axis positions, and measured coupled node lines on models of 410 wings.

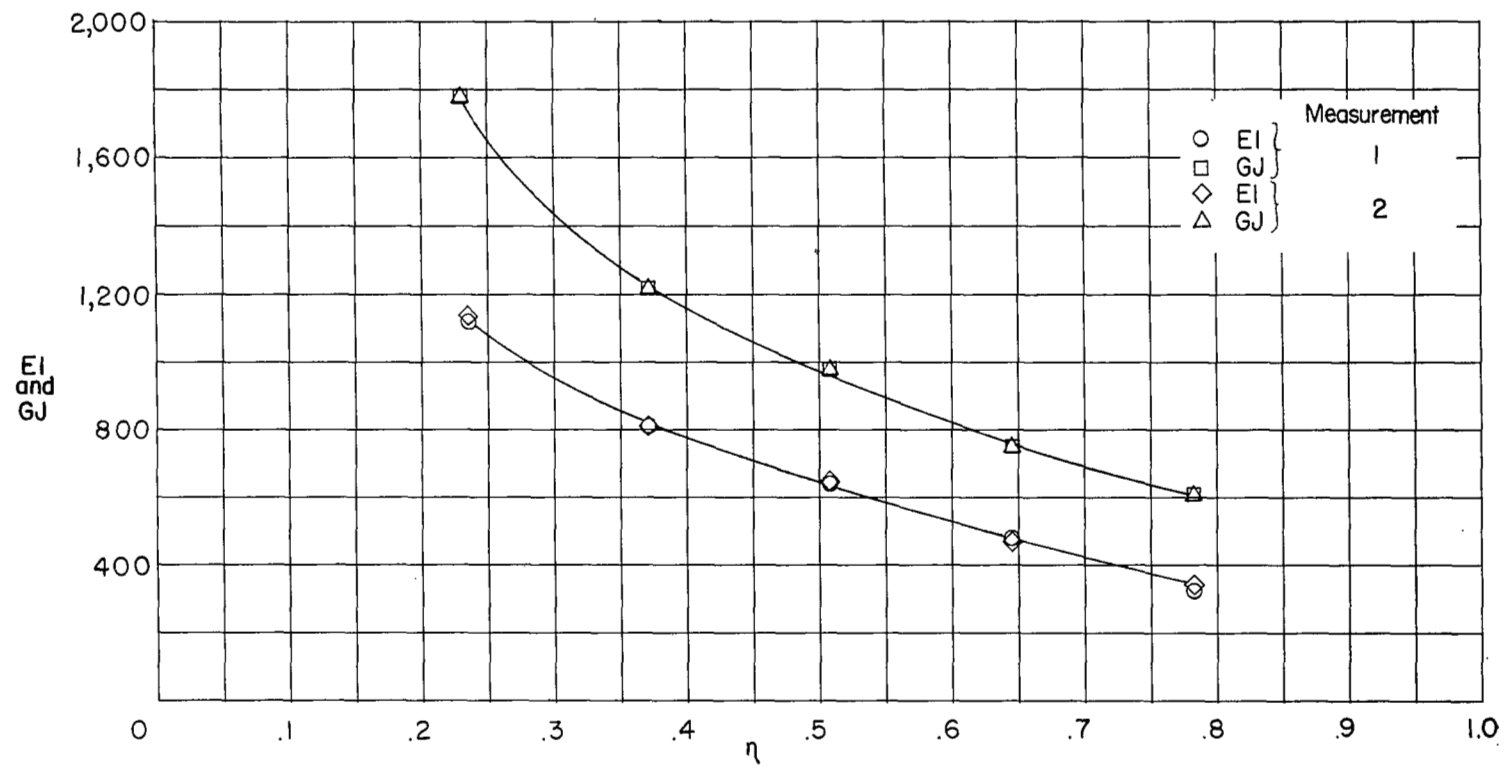


Figure 3.- Measured variation of bending and torsion stiffnesses along the span for a representative 410 wing.

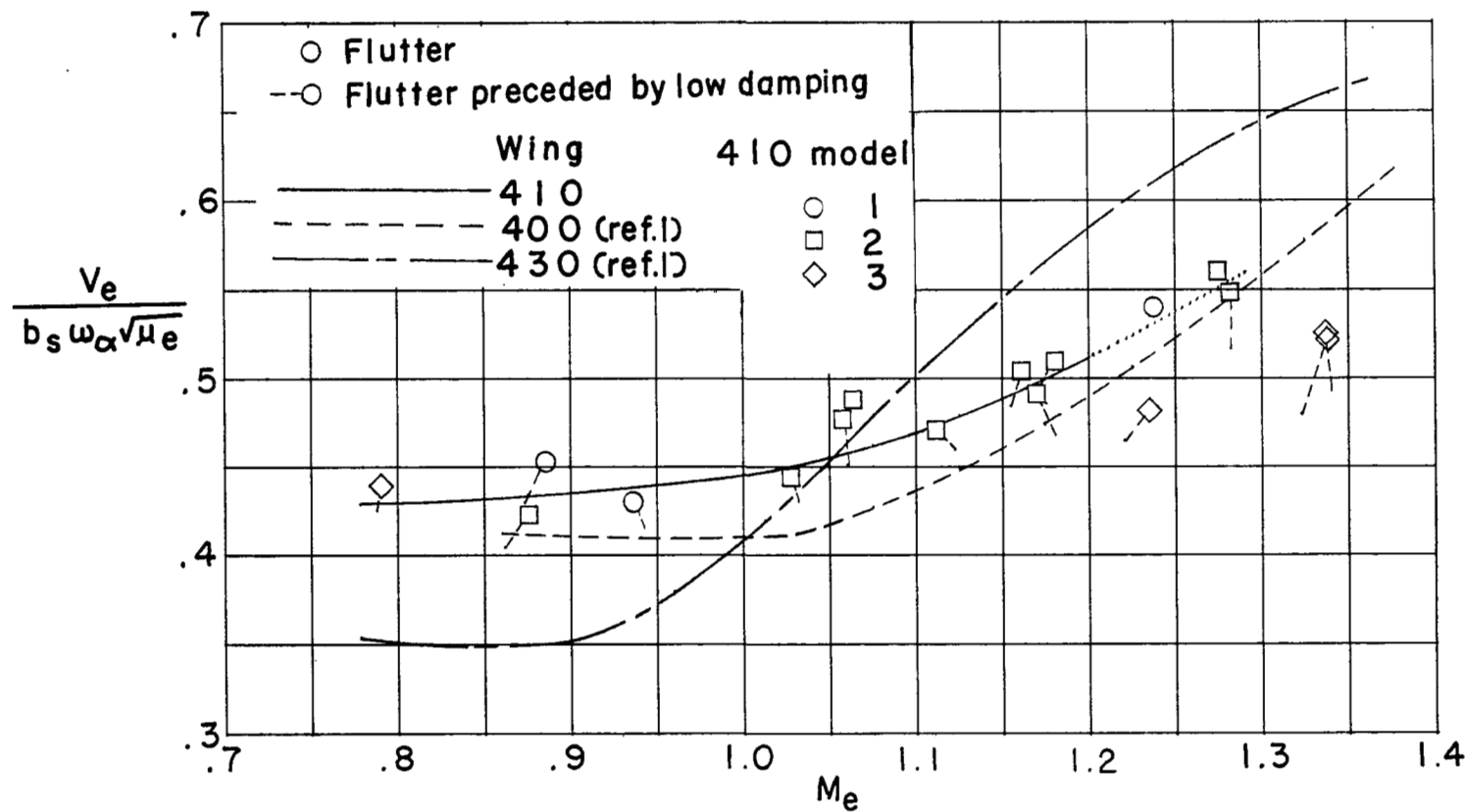


Figure 4.- Variation of parameter  $\frac{V_e}{b_s \omega_\alpha \sqrt{\mu_e}}$  with Mach number for 410, 400, and 430 wings.

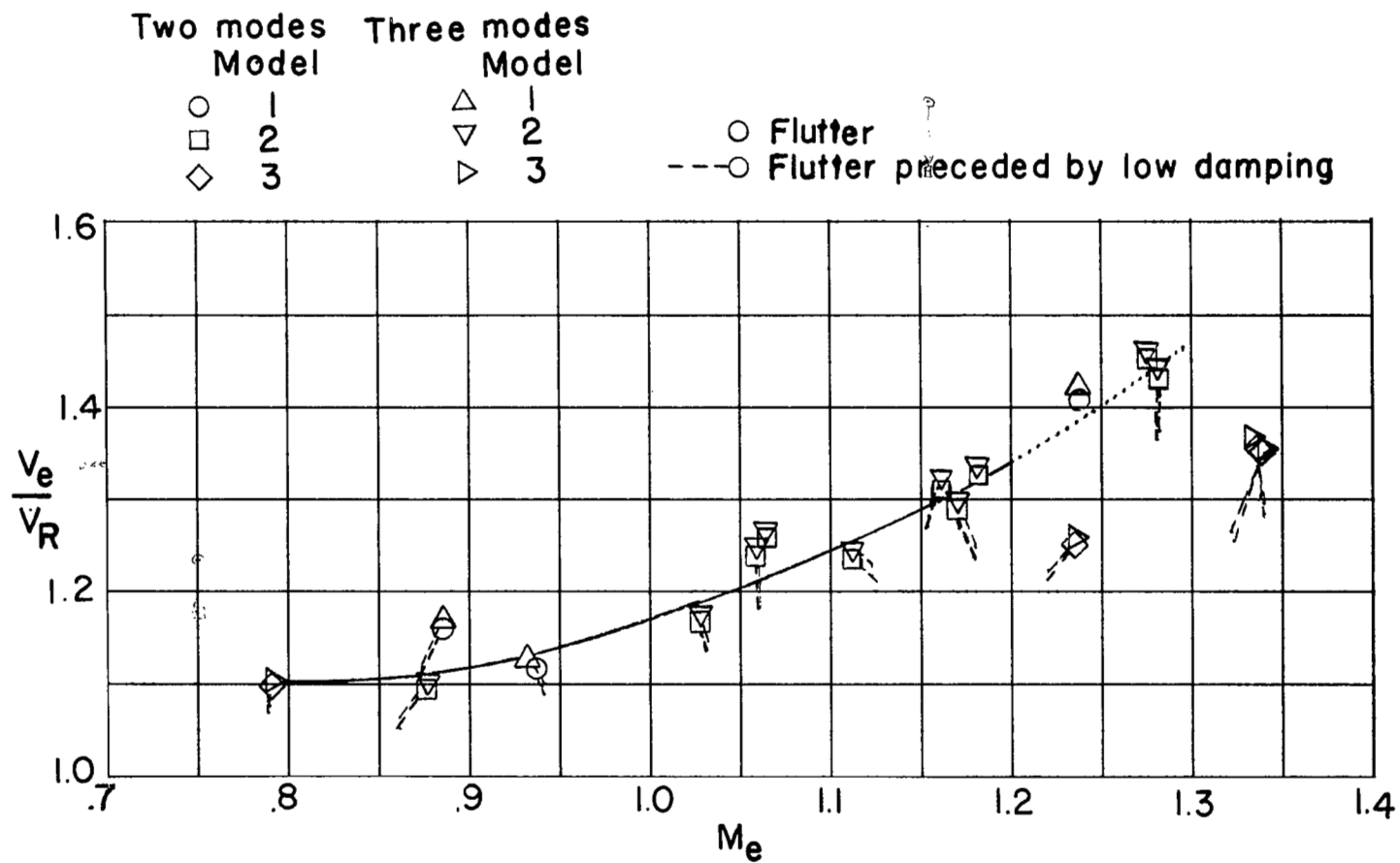


Figure 5.- Variation with Mach number of flutter-speed ratios computed for 410 wing by two-mode and three-mode analyses.

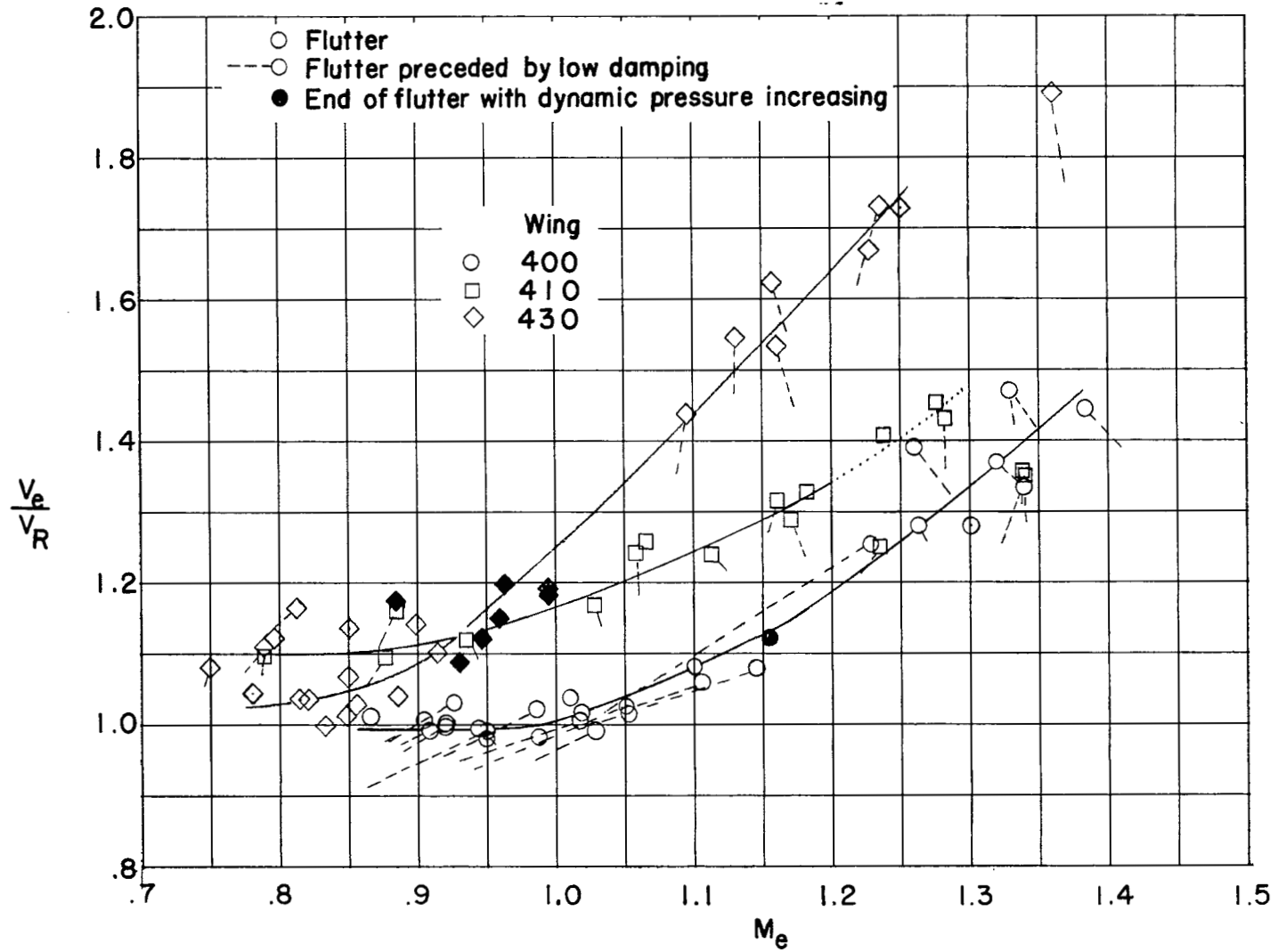


Figure 6.- Comparison of flutter-speed-ratio data for 410 wing with similar data for 400 and 430 wings of reference 1.

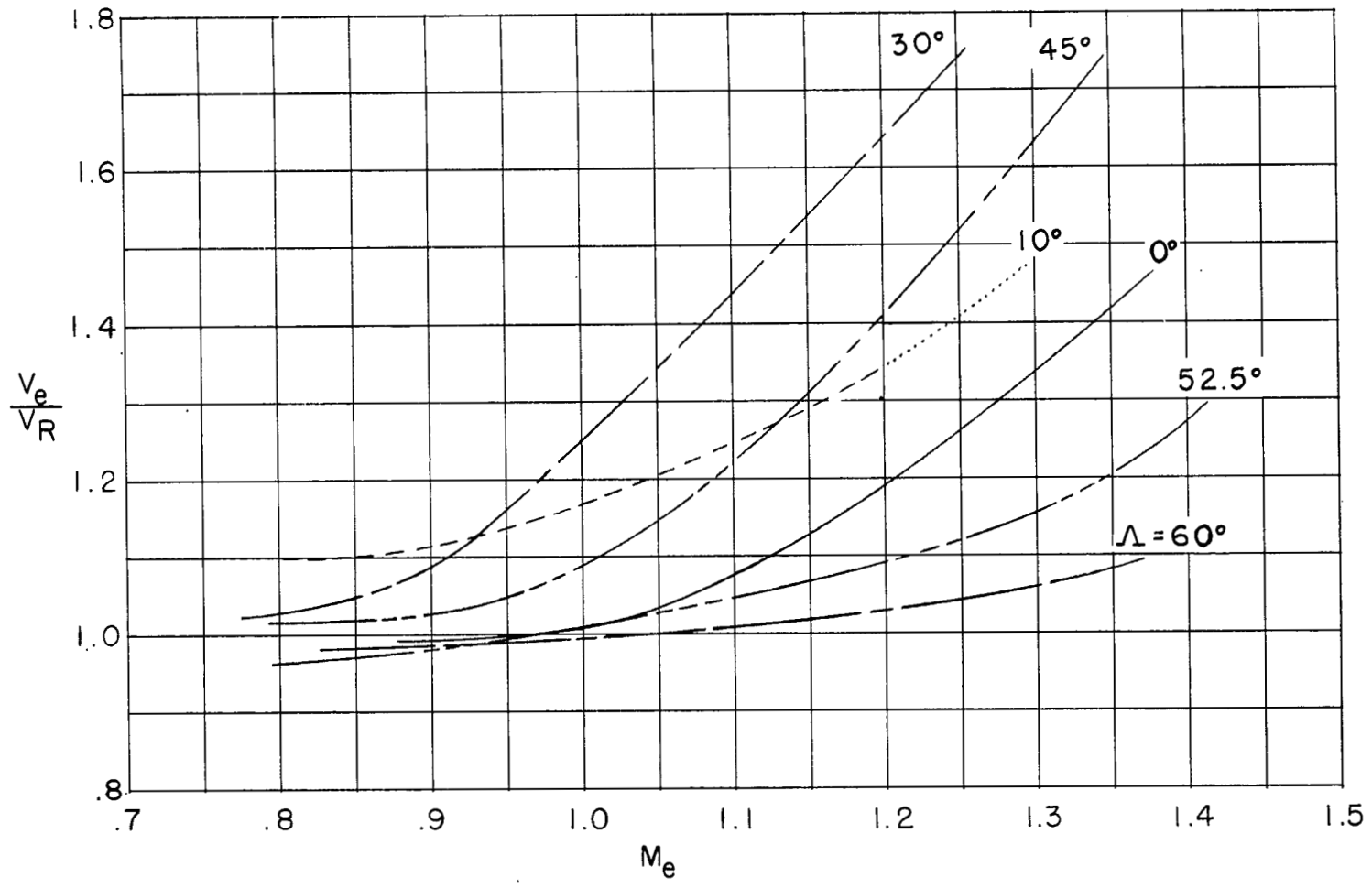


Figure 7.- Effect of sweepback on variation of flutter-speed ratio with Mach number as shown by faired flutter boundaries for 410 wing and wings of reference 1 having aspect ratios of 4 and taper ratios of 0.6.

NASA Technical Library



3 1176 01437 7296

